Journal of Alloys and Compounds 509 (2011) 2510–2517

Contents lists available at ScienceDirect

Journal of Alloys and Compounds

journal homepage: www.elsevier.com/locate/jallcom

Evolution of Ag_3Sn intermetallic compounds during solidification of eutectic Sn–3.5Ag solder

Hwa-Teng Lee*, Yin-Fa Chen

Department of Mechanical Engineering, National Cheng-Kung University, No.1, University Road, Tainan City 701, Taiwan, ROC

ARTICLE INFO

Article history:
Received 8 February 2010
Received in revised form 9 November 2010
Accepted 11 November 2010
Available online 25 November 2010

Keywords:
Ag_3Sn
Sn–3.5Ag
Cooling rate
Plate-like
Cu_6Sn_5

ABSTRACT

An experimental investigation is performed to examine the effect of the cooling rate on the morphology of the Ag_3Sn intermetallic compounds (IMCs) formed during the solidification of bulk eutectic Sn–3.5Ag solder and Sn–3.5Ag/Cu joints. It is shown that the cooling rate has a significant effect on the solidification time and therefore influences both the size and the morphology of the final Ag_3Sn compounds. Specifically, the Ag_3Sn compounds exhibit a particle-like → needle-like → needle-like with plate-like tails → plate-like → large plate-like evolution as the cooling rate is reduced. The large plate-like Ag_3Sn compounds are observed only in the Sn–3.5Ag/Cu specimens. The large plate-like Ag_3Sn formed at the interface layer due to the formation of a Cu_6Sn_5 IMC layer at the interface. Thus, it is inferred that the Cu_6Sn_5 interfacial layer in the Sn–3.5Ag/Cu specimens leads to a local enrichment of Ag at the interface and prompts the formation of large Ag_3Sn IMCs via the Cu_6Sn_5 heterogeneous nucleation sites.

1. Introduction

Eutectic Sn–3.5Ag solder has excellent mechanical and electrical properties and is therefore one of the most promising candidates for replacing conventional Sn–Pb solder [1,2]. Sn–3.5Ag solder has a eutectic point of 221 °C and contains a uniform dispersion of fine Ag_3Sn compounds, which greatly enhance its mechanical strength. However, the size and morphology of the Ag_3Sn compounds are highly sensitive to the cooling rate due to the relatively low melting point of the Sn–3.5Ag solder. According to the literature [3–5], the Ag_3Sn compounds have either a particle-like, needle-like, or plate-like (or bulk) morphology, depending on the cooling rate and Ag content. The growth of large plate-like Ag_3Sn has been widely discussed in the recent researches [5–8]. The large plate-like Ag_3Sn compounds formed in solder joints with a high Ag content or cooled at a slow cooling rate have a detrimental effect upon the mechanical performance and reliability of the joint and have therefore attracted particular attention in the literature [6–10]. In general, the formation of large Ag_3Sn plates has been attributed to the large undercooling required by the β-Sn phase to commence nucleation relative to that of the Ag_3Sn compounds, which allows the Ag_3Sn plates to nucleate and coarsen significantly before final solidification occurs [11,12].

Previous studies have shown that the Ag_3Sn compounds within eutectic Sn–3.5Ag solder cooled at a rapid cooling rate (e.g. 24 °C/s) have a fine particle-like appearance, but change to a needle-like morphology as the cooling rate is reduced [4,5,13]. However, the use of two-dimensional (2D) imagery techniques to identify the precise morphology of the Ag_3Sn compounds formed at different cooling rates is not very easy. Sidhu and Chawla [13] confirmed the presence of needle-like Ag_3Sn compounds in the Sn matrix utilizing a three-dimensional (3D) visualization method. However, the relation of the three-dimensional morphology of Ag_3Sn compounds to the cooling rate remains unclear. In order to investigate the evolution of three-dimensional Ag_3Sn compound morphology at various cooling rates, the present study fabricates bulk Sn–3.5Ag solder and Sn–3.5Ag solder/Cu specimens and then cools the specimens at four different cooling rates, namely continuous cooling, water cooling, air cooling and furnace cooling, respectively. The cooled specimens are then examined using optical microscopy (OM) and scanning electron microscopy (SEM) in order to clarify the dependence of the final size and morphology of the Ag_3Sn compounds on the cooling rate.

2. Experiment

In order to determine the evolution of Ag_3Sn intermetallic compounds in Sn–3.5Ag solder through solidification at different cooling rates, two types of experiments were used. The first experiment employed the continuous cooling method, which is similar to the Jominy end-quench test (ASTM A255) and can obtain a continuous temperature gradient, as shown schematically in Fig. 1. The cooling rates varied with distance from the bottom (the cooling source). In preparing the test sample, molten solder with a temperature of 250 °C was cast into a square tube made of 1 mm thick stainless steel and measuring 10 mm × 10 mm × 40 mm. The surface of the square tube was wrapped in an adiabatic band to ensure that heat transfer occurred only from the bottom of the tube to the bulk aluminum plate and

* Corresponding author. Tel.: +886 6 2757575x62154.
E-mail address: htlee@mail.ncku.edu.tw (H.-T. Lee).

0925-8388/$ – see front matter © 2010 Elsevier B.V. All rights reserved.
doi:10.1016/j.jallcom.2010.11.068

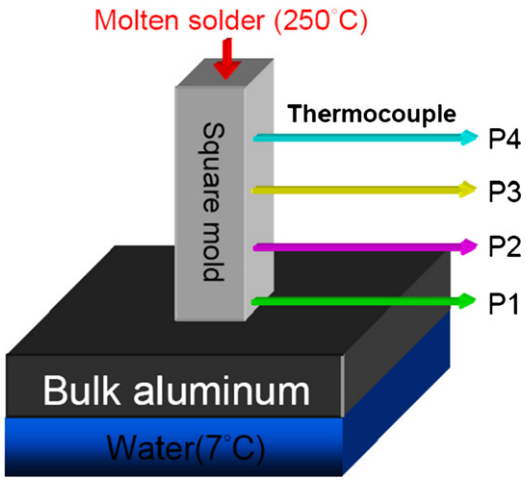

Fig. 1. Schematic illustration of continuous cooling experiment and temperature measurement positions.

cool water. The aluminum plate had dimensions of 300 mm × 100 mm × 20 mm and the cool water was maintained at a constant temperature of 7 °C. The cooling rates at four points along the length of the solder sample (P1–P4) were measured using K-type thermocouples with a diameter of 0.32 mm (American Wire Gage, AWG No. 28) spaced evenly at intervals of 10 mm. Once the solder had cooled to room temperature, it was removed from the square tube and sectioned longitudinally in order to observe the evolution of the microstructure and measure the microhardness.

In order to investigate the effect of slower cooling rates on the size and morphology of the Ag_3Sn compounds, bulk Sn–3.5Ag samples were cooled under three different cooling conditions, namely water cooling (WC), air cooling (AC) and furnace cooling (FC). To examine the effect of the Cu_6Sn_5 interfacial layer on Ag_3Sn growth, a further series of experiments was performed in which Sn–3.5Ag solder/Cu joint samples were also cooled under the WC, AC and FC cooling conditions. Fig. 2 presents a schematic diagram of the bulk solder and solder joint cooling experiment. As shown, both specimens measured 5 mm × 5 mm × 5 mm and differed only in the addition of a high-purity (99.95 wt.%) flux-coated Cu substrate with dimensions of 5 mm × 5 mm × 1 mm to the solder joint specimen. The specimens were dipped in molten solder (250 °C) for 5 s and were then allowed to cool under WC, AC or FC conditions. During the cooling process, the cooling rates of the two specimens were measured using K-type micro-thermocouples (American Wire Gage, AWG No. 28) embedded at the center of each specimen. Once the specimens had cooled to room temperature, half the specimens were sectioned and ground such that the β-Sn phases and Ag_3Sn compounds in the solder matrix could be observed using OM (Leica Metallux 3), while the remainder were deep etched in a 1:10 solution of HNO_3 and $C_2H_{50}H$, cleaned using an ultrasonic vibrator, and then observed via SEM using an FEI Quanta 400F ESEM.

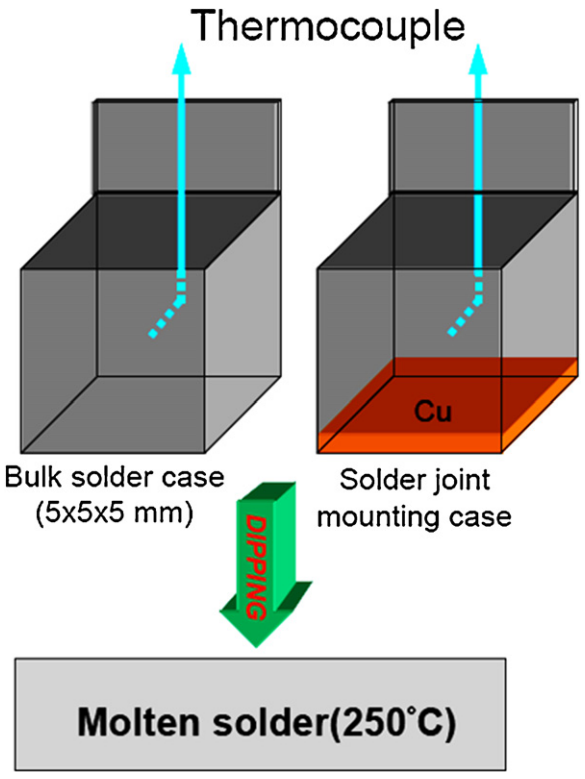

Fig. 2. Schematic illustration of bulk solder and solder joint cooling experiment and temperature measurement.

3. Results and discussion

3.1. Evolution of Ag_3Sn intermetallic compounds formed during continuous cooling

Fig. 3 illustrates the cooling curves obtained at measurement positions P1–P4 in the continuous cooling experiment. Note that the temperature history extends from the initial molten condition (250 °C) to the fully solidified condition. In general, the solder solidification process comprises four steps, namely Step 1: undercooling; Step 2: recalescence, in which nucleation of the eutectic phase commences and prompts an abrupt rise in the temperature as the result of the release of latent heat during crystal growth; Step 3: nucleation, growth and solidification, which continues until the temperature of the Sn–3.5Ag solder falls below the eutectic point; and Step 4: cooling to room temperature. The recalescence and eutectic solidification stages are clearly visible in the cooling curves obtained at measurement positions P2–P4. According to Gibbs' phase rule ($F = C - P + 1 = 2 - 3 + 1 = 0$), no degrees of freedom are left and temperature does not change in this region. Therefore, the eutectic stage appears in the cooling curve. However, the recalescence and eutectic stage cannot be seen in the cooling curve obtained at measurement position P1 since in this particular region of the solder, most of the latent heat released at the onset of eutectic phase nucleation is removed directly by the bulk aluminum and thus a local temperature rise does not occur.

As shown in Fig. 4, the cooling curves obtained at measurement positions P1–P4 can be partitioned into three discrete sections for analysis purposes. The first section extends from 250 °C molten temperature to the undercooling point. The cooling rate within this section of the curve is designated as the primary cooling rate and is annotated for convenience as CR_1. The second section of the cooling curve extends from the undercooling point to the end of solidification and defines the nucleus growth in liquid phase. This time is annotated for convenience as Gt_1. The third section of the curve extends from the end of growth to a temperature of 150 °C, i.e. the temperature below which the microstructure and IMCs in

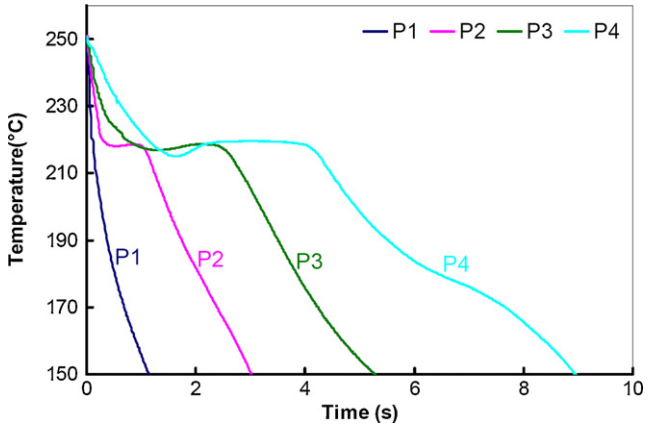

Fig. 3. Cooling curves at measurement positions P1–P4 in continuous cooling experiment.

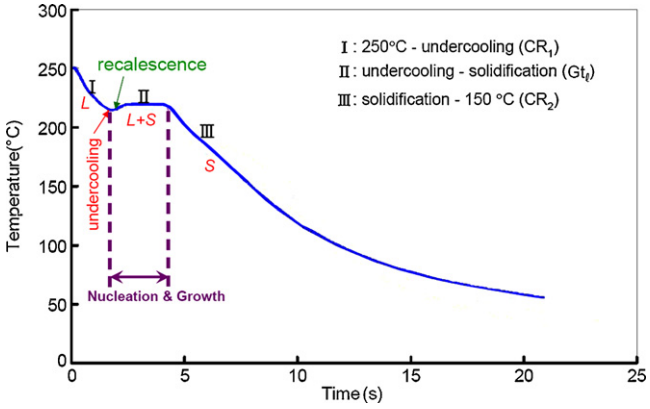

Fig. 4. Analysis of cooling curve.

Table 1
Primary and secondary cooling rates at measurement positions P1–P4 in continuous cooling experiment.

Position	P1	P2	P3	P4
CR_1 (°C/s)	263.6	116	43.9	27.1
CR_2 (°C/s)	113.6	42.1	30.8	21.6

the Sn–3.5Ag solder undergo no significant change [14]. The cooling rate within this particular portion of the curve is defined as the secondary cooling rate and is annotated for convenience as CR_2. According to the cooling record data and cooling history, the cooling rate was calculated by dividing temperature change data by its corresponding time data. In other words, the change in the temperature divided by the change in time will give an average cooling rate. The primary and secondary cooling rates obtained from the cooling curves at measurement points P1–P4 are summarized in Table 1, while the corresponding nucleation and growth times are presented in Table 2. It is noted that the cooling rates are all higher than those observed in a solder specimen cooled in a typical reflow process (average ramp-down is 6 °C/s) [15]. This result is to be expected since in the current continuous cooling experiments, the temperature within the solder is measured directly using embedded thermocouples, whereas in the reflow process, the thermocouples do not contact the solder.

Fig. 5 presents the relationship between solder microstructure and microhardness at measurement positions P1–P4 within the continuously cooled sample. It is evident that the microstructure and microhardness of the Sn–3.5Ag solder is highly sensitive to the cooling rate. Measurement position P1 is located immediately above the bulk aluminum plate (see Fig. 1), and thus when the molten solder contacted the bulk aluminum, the molten solder near the cooling source was chilled immediately. Consequently, the microstructure at P1 experiences a rapid cooling rate and a short solidification time. Thus, as shown in Fig. 5(a), the β-Sn grains in the solder microstructure have a fine, spherical appearance with an average size of just 5 μm. The cooling rate at measurement position P2 is lower than that at P1, and hence the microstructure of the solder at P2 is relatively coarser than that at P1. Thus, as shown in Fig. 5(b), the β-Sn grains have an average size of 10–20 μm. Similarly, the cooling rates at measurement positions P3 and P4 are also relatively lower than those at P1 or P2, and therefore give rise to larger β-Sn grains with an average size of 20–40 μm (see Fig. 5(c)) and 30–60 μm (see Fig. 5(d)), respectively. However, the different microstructure results in different microhardness. Fig. 5(e) shows the effect of cooing rate on microhardness at measurement positions P1–P4 in continuous cooling experiment. The microhardness of Sn–3.5Ag solder increased apparently with increasing cooling rate. With increasing cooling rate, fine β-Sn grains and Ag_3Sn compounds formed in the solder, those can benefit improving the dispersion strengthening effect in the solder matrix. Hence, the microhardness of the solder at P1 is relatively higher than others. However, the relationship between the cooling rate and the volume fraction of β-Sn phase is not clear in this study. Snugovsky et al. [16] reported that for Ag and Cu concentrations less than the Sn–Ag–Cu eutectic composition, the volume fraction of Sn dendrites increases with an increasing cooling rate, whereas for Ag and Cu concentrations greater than the Sn–Ag–Cu eutectic composition, the volume fraction tends to decrease.

Table 2
Growth time (Gt_1) at measurement positions P1–P4 in continuous cooling experiment.

Position	P1	P2	P3	P4
Gt_1 (s)	0.1	0.8	1.7	3.1

Fig. 6 presents SEM images of the Ag_3Sn compounds formed at measurement positions P1–P4 in the continuously cooled specimens. The images clearly show that both the size and the morphology of the Ag_3Sn compounds are significantly dependent on the cooling rate. P1 has the fastest cooling rate of the four measurement positions in the continuous cooling experiment. As shown in Table 1, the primary cooling rate, CR_1, has a value of 263.6 °C/s due to the proximity of point P1 to the aluminum bulk. At the completion of the solidification, the solder cools to a temperature of 150 °C at a rate of 113.6 °C/s (see Table 1). Since the solder cools so rapidly, the Ag_3Sn compounds have little time to grow, and thus the final microstructure is determined principally by the primary cooling rate and is characterized by a large number of submicron particle-like Ag_3Sn compounds with an average size of 80–900 nm.

The primary cooling rate at measurement position P2 is equal to 116 °C/s (see Table 1). Although the primary cooling rate at P2 is lower than that at P1, the growth time is still relatively short, i.e. Gt_1 = 0.8 s (see Table 2). As a result, the Ag_3Sn compounds grow only slightly compared to those formed in the solder at measurement position P1. As shown in Fig. 6(b), the solidified microstructure contains a mixture of submicron particle-like Ag_3Sn compounds with dimensions of 200–900 nm and submicron needle-like Ag_3Sn compounds with dimensions of around 0.4–1.2 μm.

The primary cooling rate at measurement position P3 is equal to 43.9 °C/s, while the growth time (Gt_1) is equal to approximately 1.7 s. In other words, the primary cooling rate is slower than that at measurement position P2 and the growth time is correspondingly increased. As a result, the Ag_3Sn compounds remain in the growth zone for longer than those near the P2 measurement position. Consequently, the Ag_3Sn compounds within the solidified microstructure are larger than those observed at either P1 or P2. As shown in Fig. 6(c), the Ag_3Sn compounds evolve from a mixture of submicron particle-like and submicron needle-like phrases at P2 to micro needle-like phases only at P3. From inspection, the needle-like Ag_3Sn compounds are found to have dimensions of approximately 10–30 μm. In addition, it is observed that the tails of some of the needle-like Ag_3Sn compounds show a slight plate-like morphology.

The primary cooling rate at measurement position P4 is equal to 27.1 °C/s, while the growth time (Gt_1) is equal to approximately 3.1 s. In other words, the cooling rate at P4 is the slowest of the four measurement positions, while the growth time is the longest. As a result, the Ag_3Sn compounds are significantly larger than those observed at measurement positions P1, P2 or P3. An inspection of Fig. 6(d) shows that the Ag_3Sn compounds have a micro needle-like morphology with an average size of approximately 20–40 μm. Furthermore, it is seen that the tails of the needle-like Ag_3Sn compounds have a distinct plate-like characteristic.

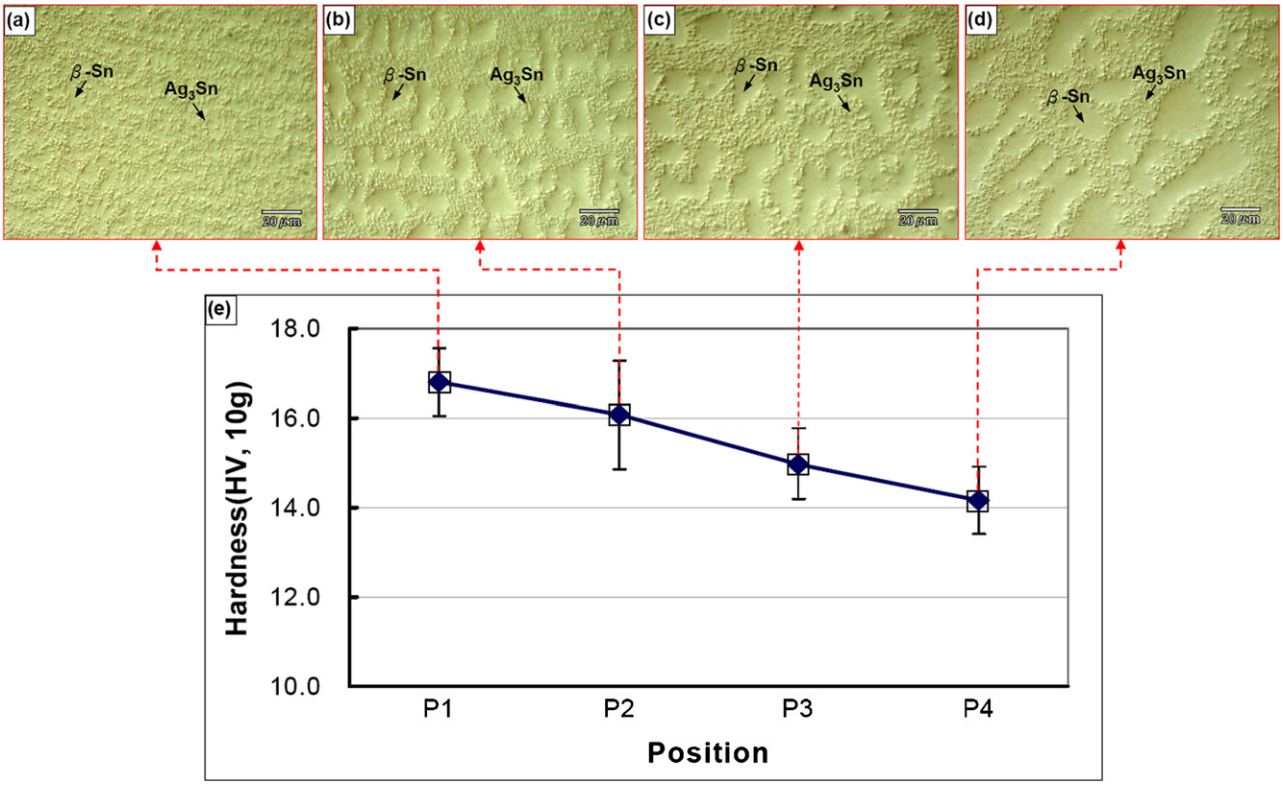

Fig. 5. Relationship between the OM microstructures and the microhardness at measurement positions P1–P4 in continuous cooling experiment: (a) P1 microstructure, (b) P2 microstructure, (c) P3 microstructure, (d) P4 microstructure, and (e) microhardness profile.

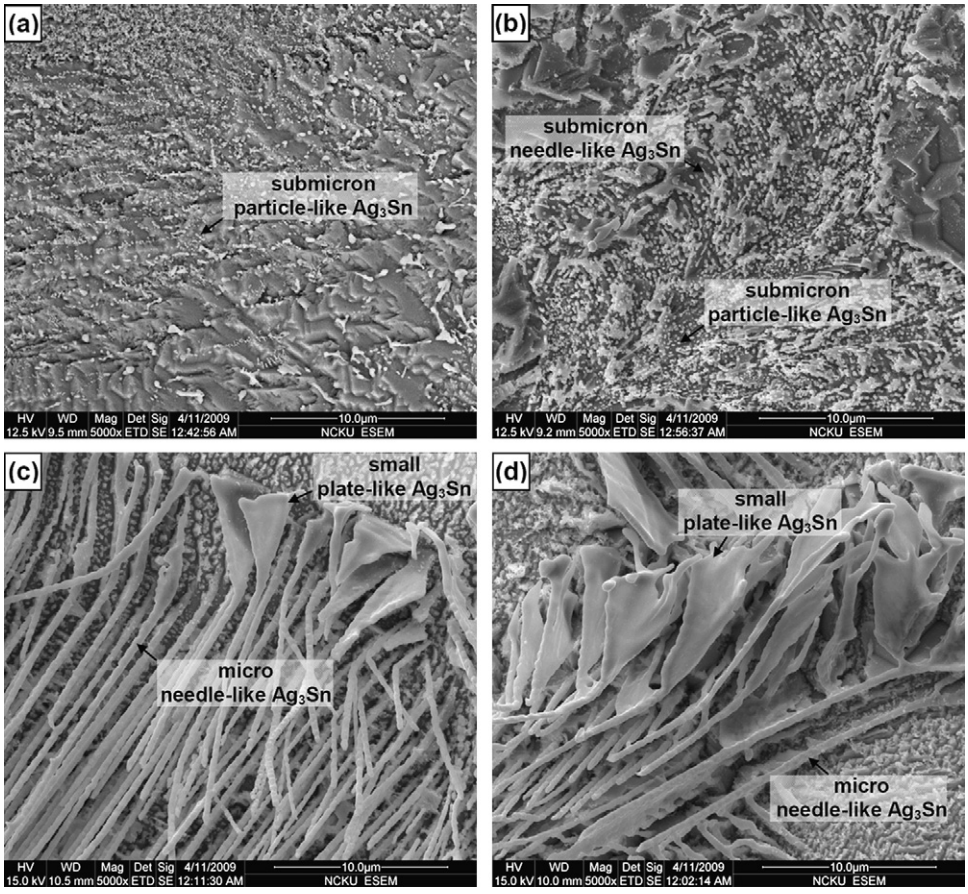

Fig. 6. 3D SEM morphologies of Ag_3Sn compounds at measurement positions P1–P4 in continuous cooling experiment: (a) P1, (b) P2, (c) P3, and (d) P4.

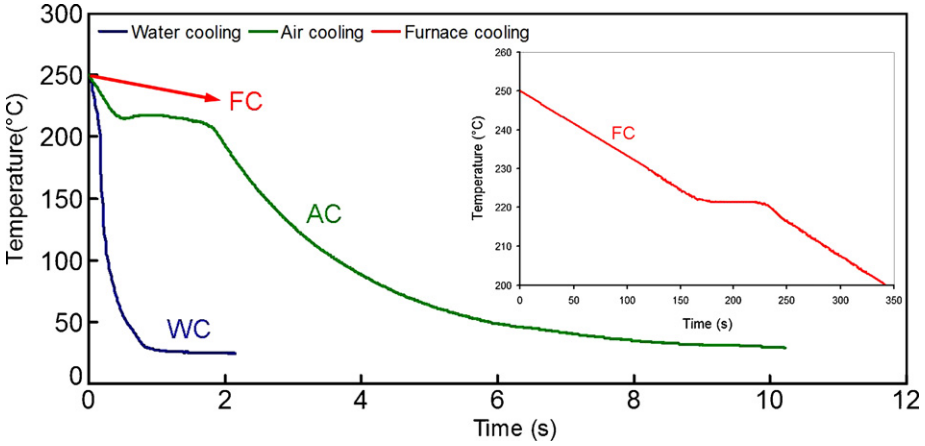

Fig. 7. Water, air and furnace cooling curves of Sn–3.5Ag bulk solder.

Overall, the results presented in Fig. 6 show that in the continuous cooling experiment, characterized by a relatively high cooling rate, the Ag_3Sn compounds transit through the following evolution as the cooling rate is reduced: submicron particle-like → submicron particle-like + submicron needle-like → micro needle-like → micro coarse needle-like with small plate-like compounds. Furthermore, it can be inferred that the microstructure is dominated by particle-like Ag_3Sn compounds in regions of the solder with a primary cooling rate of 116 °C/s or more, but contains needle-like Ag_3Sn compounds in regions of the solder with a lower primary cooling rate. Based on our results, it is clear that the morphology of Ag_3Sn compounds is significantly affected by the cooling condition. The Ag_3Sn compounds coarsen with increased growth time. The driving force for the crystal growth of Ag3Sn compounds can be described as a diffusion-controlled growth mechanism. Faster cooling rates promote nucleation but suppress the growth of Ag_3Sn, yielding a submicron particle-like and submicron needle-like Ag_3Sn. Conversely, slower cooling rates result in comparatively coarse needle-like and plate-like Ag_3Sn in micro scale. In addition, the needle-like Ag_3Sn that forms during a slower cooling rate appears to have a preferred orientation within individual Sn grains. The needle-like grains can grow along a given crystallographic orientation, which is given by the smallest misfit strain between the Ag_3Sn crystal and the Sn grains [17]. As discussed above, it can be summarized that the evolution and formation of Ag_3Sn morphology are closely related to cooling rate and Sn grain orientation.

Comparison of these SEM micrographs with the OM micrographs in Fig. 5 reveals that the etching process exposed the real 3D morphology of Ag_3Sn IMC. However, the 3D morphology of Ag_3Sn IMC appears to differ from the 2D morphology of OM micrographs in the same sample, as in the 2D OM micrograph, the morphology of the Ag_3Sn compounds appears to be particle-like. However, it should be noted that the OM micrograph is not a complete micrograph of Ag_3Sn IMC. Therefore, using the complete 3D morphology to define the micrograph of Ag_3Sn provided a more accurate representation. The SEM micrographs presented in Fig. 6 show that the deep etching process results in the removal of the β-Sn phases from the solder matrix, leaving the Ag_3Sn compounds exposed. As a result, the SEM micrographs capture the true 3D morphology of the various Ag_3Sn compounds. By contrast, the OM micrographs presented in Fig. 5 present only the 2D morphology of the various compounds. As a result, the OM images incorrectly suggest that all the Ag_3Sn compounds have a particle-like morphology. In other words, to correctly identify the effect of the cooling rate on the morphology of the Ag_3Sn compounds, it is necessary to use some form of 3D visualization method.

3.2. Evolution of Ag_3Sn intermetallic compounds formed during water, air and furnace cooling

The continuous cooling method provides a continuous temperature gradient within the bulk solder specimen and allows the continuous transition of the Ag_3Sn compounds to be observed. However, it provides a relatively high cooling rate in all regions of the specimen (see Table 1). To clarify the effects of slower cooling rates on the size and morphology of the Ag_3Sn compounds formed within the Sn–3.5Ag solder during solidification, bulk solder specimens were cooled under water cooling (WC), air cooling (AC) and furnace cooling (FC) conditions, respectively. Fig. 7 presents the cooling curves obtained during the WC, AC and FC cooling experiments and shows that the water cooling method yields the highest cooling rate, while the furnace cooling method yields the lowest.

The primary cooling rates for each cooling condition are indicated in Table 3, while the corresponding nucleation and growth times are presented in Table 4. It can be seen that the primary cooling rate in the WC bulk solder sample is approximately 223.1 °C/s (CR_1), giving a growth time (Gt_1) of about 0.2 s. Meanwhile, the primary cooling rate in the AC bulk solder sample is around 80.6 °C/s (CR_1), leading to a growth time (Gt_1) of approximately 1.2 s. Finally, the primary cooling rate in the FC sample is about 0.2 °C/s (CR_1), giving a growth time (Gt_1) of around 55.4 s. The SEM images presented in Figs. 8–10 show that the primary cooling rate and nucleation time have a significant effect on the morphology of the Ag_3Sn compounds. For example, Fig. 8 shows that the eutectic region of the WC sample comprises many submicron particle-like Ag_3Sn compounds with an average size of around 100–950 nm. Meanwhile, in the AC sample, characterized by a lower cooling rate, the Ag_3Sn compounds have a micro needle-like morphology, as shown in Fig. 9. Finally, Fig. 10 shows that the extremely slow cooling rate in the FC sample delays the time for which the Ag_3Sn compounds remain within the growth region and therefore prompts the formation of micro plate-like Ag_3Sn compounds. The plate-like compounds

Table 3
Primary cooling rates in bulk solder cooled in water, air and furnace.

Cooling condition	WC	AC	FC
CR_1 (°C/s)	223.1	80.6	0.2

Table 4
Growth time (Gt_1) of bulk solder cooled in water, air, and furnace.

Cooling condition	WC	AC	FC
Gt_1 (s)	0.2	1.2	55.4

Fig. 8. 3D SEM morphology of Ag_3Sn compounds in WC bulk solder.

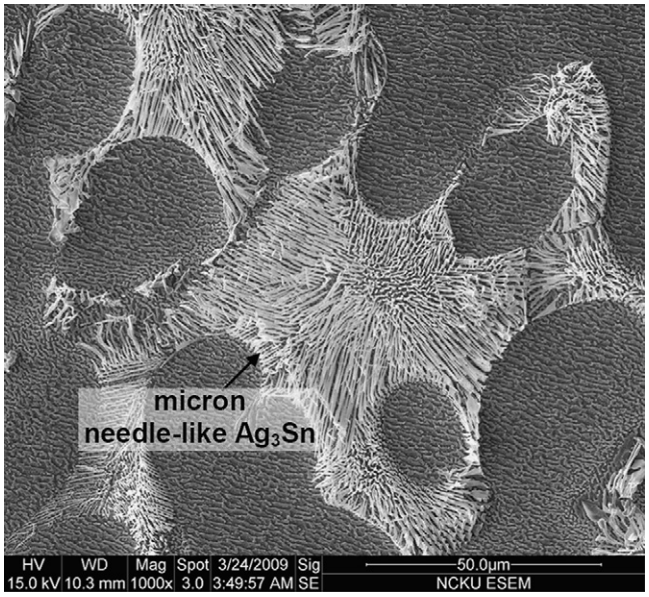

Fig. 9. 3D SEM morphology of Ag_3Sn compounds in AC bulk solder.

have one of two different forms, namely leaf-like (see Fig. 10(a)) or conventional plate-like (see Fig. 10(b)). As discussed in Section 3.1, the micro needle-like Ag_3Sn compounds formed in the Sn–3.5Ag solder under continuous cooling tend toward a coarse needle-like morphology with plate-like tails as the cooling rate is reduced (see Fig. 6(c) and (d)). The images presented in Fig. 10 suggest that the extremely low cooling rate induced in the FC specimen prompts a further transformation of these needle-like compounds and plate-like tails as a result of atomic diffusion during the solidification process. It can be speculated that the coarse needle-like compounds and the small plate-like tails of Ag_3Sn compounds grew into leaf-like Ag_3Sn IMC. The other kind of plate-like Ag_3Sn compound appeared in the region of needle-like Ag_3Sn compounds, as shown in Fig. 10(b). It can be speculated that the plate-like Ag_3Sn compound combined with the needle-like Ag_3Sn compounds in the eutectic region. Specifically, it seems that some of the coarse needle-like compounds and small plate-like tails grow into leaf-like Ag_3Sn compounds in their own right, while others coalesce with one another to form relatively large plate-like Ag_3Sn compounds.

3.3. *Effect of Cu on Ag_3Sn intermetallic compounds formed during furnace, air, and water cooling*

Fig. 11 presents SEM micrographs of the microstructures of the Sn–3.5Ag solder/Cu joints following the WC, AC and FC cooling processes. Note that Fig. 11(a)–(c) show the microstructures of the WC, AC and FC samples far from the Cu_6Sn_5 interfacial layer, while Fig. 11(d)–(f) show the microstructures of the corresponding samples close to the Cu_6Sn_5 interfacial layer. Comparing the two sets of figures, it is evident that the β-Sn grains distant from the interfacial layer are noticeably larger than those near the interfacial layer. This result is consistent with the finding in [18] that the Cu substrate dissolves in eutectic Sn–Ag solder and prompts a nucleation of the β-Sn dendrites. In addition, it is seen that the morphologies of the Ag_3Sn compounds distant from the interfacial layer in the WC, AC and FC solder joint samples (Fig. 11(a)–(c)) are similar to those in the WC, AC and FC bulk solder samples (see Figs. 8–10). In other words, the Ag_3Sn compounds distant from the interfacial layer in the WC, AC and FC solder joint samples have particle-like, needle-like, and plate-like morphologies, respectively. However, the Ag_3Sn compounds near the Cu_6Sn_5 interfacial layer in the WC, AC and FC samples are significantly larger than those distant from the interfacial layer, as shown in Fig. 11(d)–(f). This coarsening effect is particularly evident in the FC solder joint, and results in the formation of large, plate-like Ag_3Sn compounds adjacent to the Cu_6Sn_5 interfacial layer. From inspection, the thickness and length

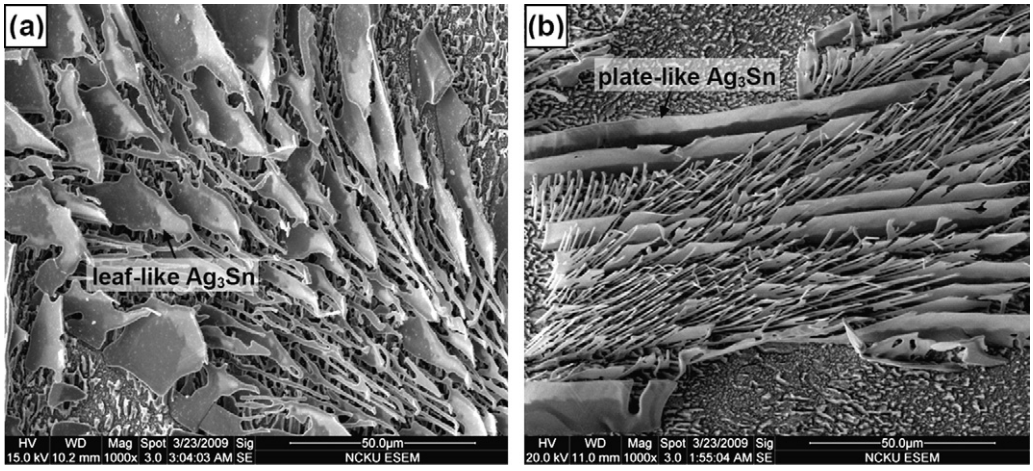

Fig. 10. 3D SEM morphologies of Ag_3Sn compounds in FC bulk solder: (a) leaf-like and (b) plate-like.

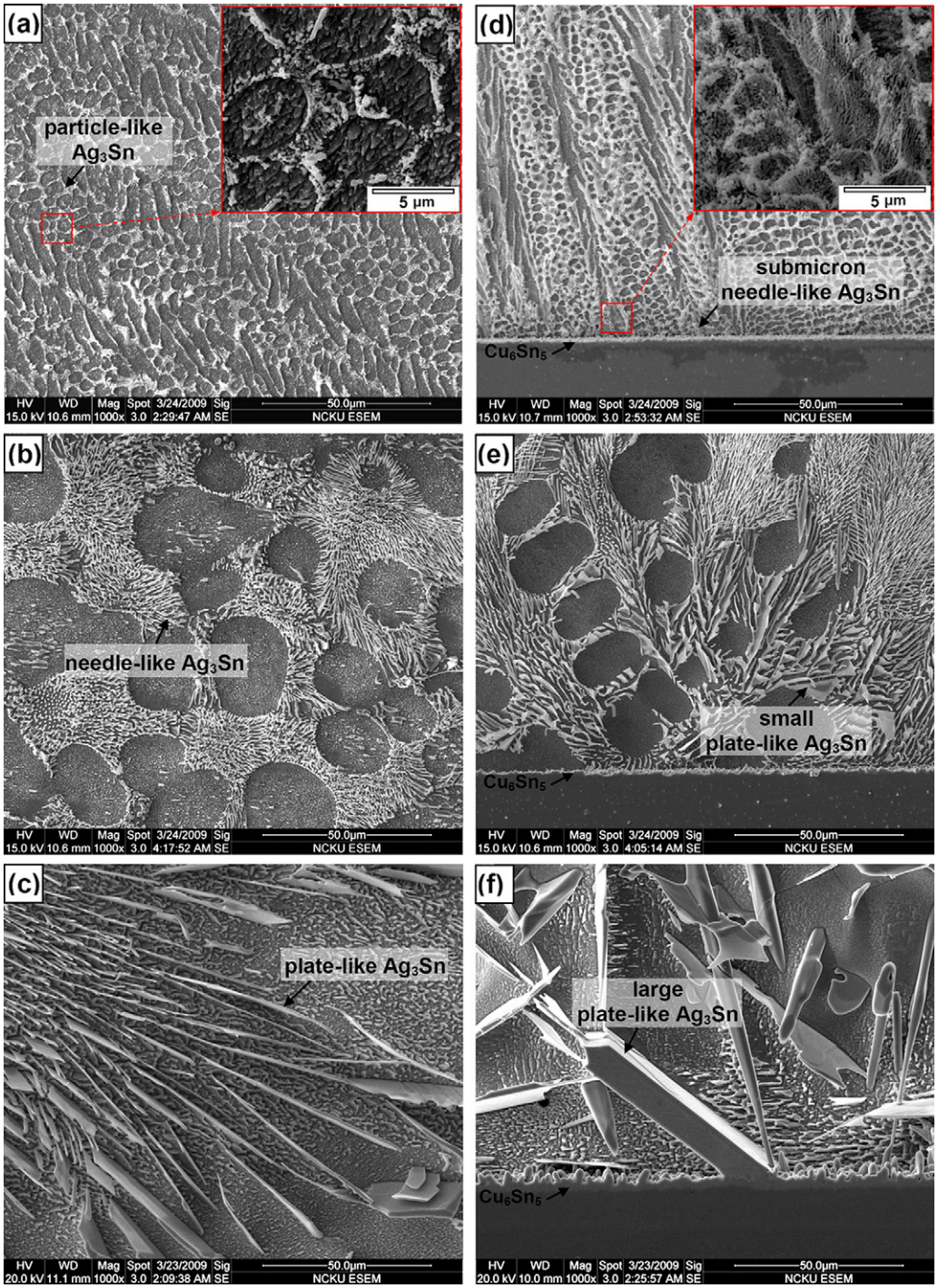

Fig. 11. Microstructures of solder joint samples distant from interfacial layer: (a) WC, (b) AC, and (c) FC; and close to interfacial layer: (d) WC, (e) AC, and (f) FC.

of the Ag_3Sn compound is found to be around 5 μm and 50 μm, respectively. Significantly, the large plate-like Ag_3Sn compound is absent in the bulk solder samples cooled under equivalent cooling conditions. Hence the Cu_6Sn_5 interfacial layer grows before the liquid solder solidification occurs during the soldering process. The composition of liquid solder at the liquid/Cu_6Sn_5 interface should acquire a value that the liquid is in local equilibrium with Cu_6Sn_5. This value is not the original solder composition [19]. Therefore, it seems that the formation of the plate-like compounds is caused by the presence of the Cu_6Sn_5 interfacial layer, which prompts a depletion of the Sn content in the local region of the solder microstructure and leads to a corresponding enrichment in the local Ag content as a result. As reported in [10,20,8], the presence of a high Ag content has a clear effect on promoting the nucleation and formation of large plate-like Ag_3Sn IMCs. Therefore, primary Ag_3Sn crystals form near the Cu_6Sn_5 interfacial layer during the initial stages of the solidification process. An increase of the local concentration of Ag will be balanced to a eutectic composition after the formation of primary Ag_3Sn, which grows rapidly within the liquid phase before final solidification. In the FC sample, the solidification time is significantly longer than that in the WC or AC samples, and thus the primary Ag_3Sn compounds have sufficient time to grow into a large plate-like morphology. In addition, Cu atoms in undercooled solder alloy prompt the nucleation of large Ag_3Sn plates

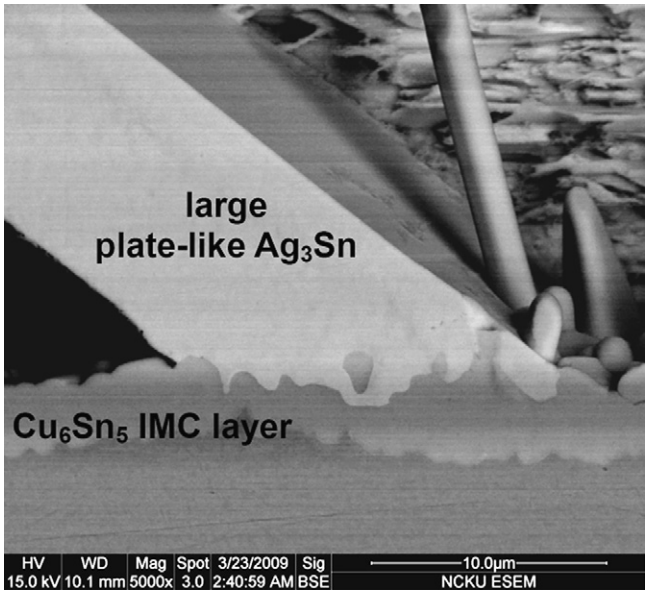

Fig. 12. High-magnification backscattered electron image of FC interface microstructure between the large plate-like Ag_3Sn compound and Cu_6Sn_5 IMC layer.

[12]. Some previous studies have reported that the Cu_6Sn_5 interfacial layer is a good energy-preferential heterogeneous nucleation site for Ag_3Sn [21,22]. Fig. 12 presents the large plate-like Ag_3Sn compound resided at the scallop-type Cu_6Sn_5 compound surface. It means that Cu_6Sn_5 IMC layer can provide heterogeneous nucleation sites for Ag_3Sn compounds. In other words, Ag_3Sn compounds are formed adjacent to the interfacial layer in order to reduce the interfacial energy. Overall, it can be inferred that the presence of the large plate-like Ag_3Sn compounds in the Sn–3.5Ag solder/Cu joints is caused by the formation of the Cu_6Sn_5 interfacial layer, which prompts an increase in the local Ag content and, via the effects of IMC layer, serves as a heterogeneous nucleation site for the Ag_3Sn compounds.

4. Conclusions

This study has performed an experimental investigation into the effect of the cooling rate on the size and morphology of the Ag_3Sn compounds formed in bulk Sn–3.5Ag solder and Sn–3.5Ag solder/Cu joints cooled under four different cooling conditions, namely continuous, water cooling, air cooling, and furnace cooling. The morphologies of the Ag_3Sn compounds have been observed using both 2D (OM) and 3D (SEM) imaging techniques. The experimental results support the following major conclusions:

Four basic types of Ag_3Sn compound are formed in the Sn–3.5Ag solder during solidification at different cooling rates, namely particle-like, needle-like, plate-like, and large plate-like.

During the solidification process, the cooling rate determines the growth time (Gt_1) and therefore affects both the size and the morphology of the Ag_3Sn compounds. The Ag_3Sn compounds coarsen with an increasing growth time, the evolution of the Ag_3Sn compound morphology as the cooling rate is reduced can be summarized as follows: submicron particle-like → submicron needle-like → micro needle-like → micro coarse needle-like with plate-like tails → plate-like → large plate-like.

The large plate-like Ag_3Sn compounds formed only at the interface layer in Sn–3.5Ag solder due to the formation of a Cu_6Sn_5 IMC layer at the interface. When the Cu_6Sn_5 IMC layer formed, the Sn concentration decreased and provided the heterogeneous nucleation sites at the interface. This result indicates enrichment of Ag at the interface, with a primary Ag_3Sn form in liquid phase. Therefore, the large plate-like Ag_3Sn can grow rapidly within the liquid phase before final solidification of the solder joint.

Acknowledgment

The authors would like to thank National Science Council for the financial support of this work under the contract of No. NSC 97-2221-E-006-021-MY3.

References

[1] ESPEC Technology Report, 1, 2002.
[2] M. Abtew, G. Selvaduray, Mater. Sci. Eng. R. Rep. 27 (2000) 95–141.
[3] F. Ochoa, X. Deng, N. Chawla, J. Electron. Mater. 33 (2004) 1596–1607.
[4] J.M. Song, J.J. Lin, C.F. Huang, H.Y. Chuang, Mater. Sci. Eng. A. Struct. Mater. 466 (2007) 9–17.
[5] D.W. Henderson, T. Gosselin, A. Sarkhel, J. Mater. Res. 17 (2002) 2775–2778.
[6] K.S. Kim, S.H. Huh, K. Suganuma, J. Alloys Compd. 352 (2003) 226–236.
[7] H.T. Lee, Y.F. Chen, T.F. Hong, K.T. Shih, IEEE Proceedings of Electronics Packaging Technology Conference, Singapore, 2009, P0304.
[8] J. Shen, Y.C. Chan, S.Y. Liu, Intermetallics 16 (2008) 1142–1148.
[9] K.S. Kim, S.H. Huh, K. Suganuma, Mater. Sci. Eng. A. Struct. Mater. 333 (2002) 106–114.
[10] S.K. Kang, W.K. Choi, D.Y. Shih, D.W. Henderson, T. Gosselin, A. Sarkhel, C. Goldsmith, K.J. Puttlitz, JOM 55 (2003) 61–65.
[11] I. Ohnuma, M. Miyashita1, K. Anzai, X.J. Liu1, H. Ohtani, R. Kainuma, K. Ishida, J. Electron. Mater. 29 (2000) 1137–1144.
[12] K.W. Moon, W.J. Boettinger, U.R. Kattner, F.S. Biancaniello, C.A. Handwerker, J. Electron. Mater. 29 (2000) 1122–1136.
[13] R.S. Sidhu, N. Chawla, Scripta Mater. 54 (2006) 1627–1631.
[14] Q. Hu, Z.S. Lee, Z.L. Zhao, D.L. Lee, IEEE Proceedings of International Conference on Asian Green Electronics, 2005, pp. 156–160.
[15] JEDEC Standard J-STD-020C, Moisture/Reflow Sensitivity Classification for Nonhermetic Solid State Surface Mount Devices, 2004.
[16] L. Snugovsky, P. Snugovsky, D.D. Perovic, J.W. Rutter, Mater. Sci. Technol. 21 (2005) 61–68.
[17] R.S. Sidhu, S.V. Madge, X. Deng, N. Chawla, J. Electron. Mater. 36 (2007) 1615–1620.
[18] S. Chada, R.A. Fournelle, W. Laub, D. Shangguan, J. Electron. Mater. 29 (2000) 1214–1221.
[19] H. Yu, J.K. Kivilahti, IEEE Proceedings of International Conference on Component and Packaging Technologies, 2006, pp. 778–786.
[20] Y. Lu, H. Balkan, K.Y. Simon Ng, J. Mater. Sci. Mater. Electron. 17 (2006) 171–188.
[21] D.Q. Yu, L. Wang, C.M.L. Wu, C.M.T. Law, J. Alloys Compd. 389 (2005) 153–158.
[22] H.W. Tseng, C.Y. Liu, Mater. Lett. 62 (2008) 3887–3889.